JOURNAL OF MATERIALS SCIENCE 30 (1995) 5691–5699

Dissolution kinetics of glass fibres in saline solution: *in vitro* persistence of a sparingly soluble aluminium-rich leached layer

P. BAILLIF*, B. CHOUIKHI, L. BARBANSON, J. C. TOURAY
URA CNRS 1366 Université d'Orléans, Ecole Supérieure de l'Energie et des Matériaux, Rue Léonard de Vinci, 45072-Orléans Cedex 2, France

The dissolution of boro-silicate glass fibres in physiological saline solution was studied at 37 °C either in a non-refilled or in a periodically refilled reactor. Large variations of the weight losses were observed with time and refilling frequencies. The weight losses were found to increase with the refilling frequency. Sections of altered fibres, studied using scanning electron microscopy, show an outer hydrated layer surrounding an unaltered glass core. The residual silicon- and aluminium-rich hydrated layer (Al/Si = 0.2, H_2O/Al = 16–19) was characterized by X-ray photoelectron spectrometry, energy dispersive spectrometry and thermogravimetric analysis. The thickness of the hydrated layer may be theoretically calculated from the degree of reaction progression. Under unsteady state conditions, most of the dissolution occurs at the fresh glass–hydrated layer boundary, through selective processes. The proposed model explains the persistence of the aluminium-rich residue when dissolution proceeds in non-replenished systems.

1. Introduction

Estimations of the biodurability of man-made mineral fibres (MMMF) are important to select harmless materials [1]. Because of the high cost of *in vivo* experiments, most of these determinations are usually carried out *in vitro* [2–9] using physiological saline solutions. An objective of this work was to study the dissolution kinetics and mechanisms of boron-rich siliceous glass fibres, chosen as a model of biodegradable MMMF, in order to understand the persistence of sparingly soluble residues.

In acid and neutral solutions, the dissolution of silicate glasses under steady-state conditions results in the formation of a leached layer, whose thickness intrinsically depends on the composition of these materials [10–17]. Dissolution is either transport- or reaction-controlled [18–21] and modelling must take into account the following processes: (i) selective dissolution at the hydration front, at the bottom of the leached layer; (ii) dissolution of the leached layer through surface reactions; (iii) transport in the solution; and (iv) transport by diffusion through the leached layer.

Unfortunately, any quantitative global approach depends on a number of hypotheses and mathematical simplifications and most interpretations are limited to the modelling of the surface reaction (process ii) using the transition-state theory [22–26].

A general consequence of the data presented in this paper is to demonstrate, through a kinetic experimental study and a mass-balance interpretation, that under unsteady state conditions, the solubilization of a silicate glass occurs mostly through selective leaching (process i) while congruent dissolution of the leached layer (process ii) is inhibited by silica diffusing to the solution from the hydration front.

2. Materials and methods

Experiments were performed with a relatively rapidly dissolving glass (referred to as CM44), whose composition (Table I) is derived from that of an insulation glass. The fibres of uniform diameter 10.0 ± 1.0 μm, were obtained by a textile process (courtesy of Saint-Gobain Recherche, Aubervilliers, France).

The dissolution of the glass fibres was investigated at 37 ± 1 °C in a physiological saline solution (Table II) derived from the Gamble solution [27] and developed by Kanapilly *et al.* [28]. This solution, previously used by Feck [29] and Leineweber [30], was poorer in calcium ions than that used by Scholze and Conradt [7]. Its initial pH ranged from 7.6–8.0. To prevent the growth of microorganisms, 0.5 ml formaldehyde was added per litre of solution.

Investigations were carried out using two experimental leaching devices. The first one used successive batches (experiments in static mode referred to as ST) while the second one had been designed to periodically renew the solution (experiments in periodic refilling mode). In both leaching modes, fragments of

*Author to whom all correspondence should be sent.

0022–2461

TABLE I Chemical composition (wt %) of the investigated glass fibres (CM44)

SiO_2	CaO	Al_2O_3	B_2O_3	Na_2O	P_2O_5	MgO
61	7	1	11	16	1	3

fibres about 2 cm long were laid on a teflon grid within a teflon reactor. The weight of the fibres was 30.0 ± 0.1 mg and the volume of the solution was 250 ml. The runs were performed from 1–28 days (one static experiment at 60 days). After each run, the fibres were removed from the solution, then rinsed with deionized water and dried at 37 °C for 24 h in an oven before weighing.

In static mode the reactors were placed in an oven regulated at 37 ± 1 °C. The collected solutions were filtered with a 0.22 μm pore diameter filter then poured in tubes and stored in a freezer before their chemical analysis by atomic absorption spectrometry (AAS).

In periodic refilling mode (without stirring and referred to as R(x), or with stirring and referred to as RA(x), where x is the renewal frequency in days^{-1}) the reactors were immersed in a water bath regulated at 37 ± 1 °C (Fig. 1). Each reactor was closed with a cover fitted with four apertures ensuring different operations, such as draining, filling and venting of the reactor and pH measurement. The preheated solution was delivered from a container by a peristaltic pump. During some runs, the solutions were stirred in the reactor with a magnetic stirrer. The device used was fitted with solenoid valves and time-switches to provide setting capabilities in the frequency of the renewal of the solution. The cycle time was fixed to 20, 60, 160 and 480 min corresponding to the following frequencies of 72, 24, 9 and 3 cycles per day.

The pH was measured after each run for the static mode and during the experiments for the second mode. Fibre diameter measurements and energy dispersive spectroscopy (EDS) analysis were performed on polished sections of fibres included in epoxy resin, using scanning electron microscopy (SEM). The surface composition of the altered fibres was obtained by X-ray photoelectron spectroscopy (XPS) analysis.

3. Results

3.1. pH variation

For the static mode experiments, a slight increase of the pH at 8.3 ± 0.3 was observed, probably resulting from the transfer of "modifiers" from the glass to the solution. By contrast, in all the runs with periodic refilling of the reactor, the pH remained constant at 7.6 ± 0.2 because of the short duration of the cycles which limited ionic concentrations in the solution.

3.2. SEM observations

SEM observations performed on the polished sections of the altered fibres display an hydrated layer surrounding an unaltered circular core (Fig. 2a). With increasing time, the diameter of the circular core decreases, the thickness of the hydrated layer increases and the bulk diameter (unaltered core + hydrated layer) of the fibres decreases. A similar variation of the diameters is observed, for the same run duration, at increasing renewal frequencies with periodic refilling

TABLE II Composition (g l^{-1}) (H_2SO_4 in μl) of the simulated extracellular solution; pH = 7.6 ± 0.2. To prevent the growth of algae or bacteria, 0.5 ml^{-1} formaldehyde was added

NaCl	$NaHCO_3$	Na_3–Cit–$3H_2O$	Glycine	NH_4Cl	NaH_2PO_4–$2H_2O$	$CaCl_2$–$2H_2O$	H_2SO_4
6.78	2.26	0.06	0.45	0.53	0.16	0.03	30

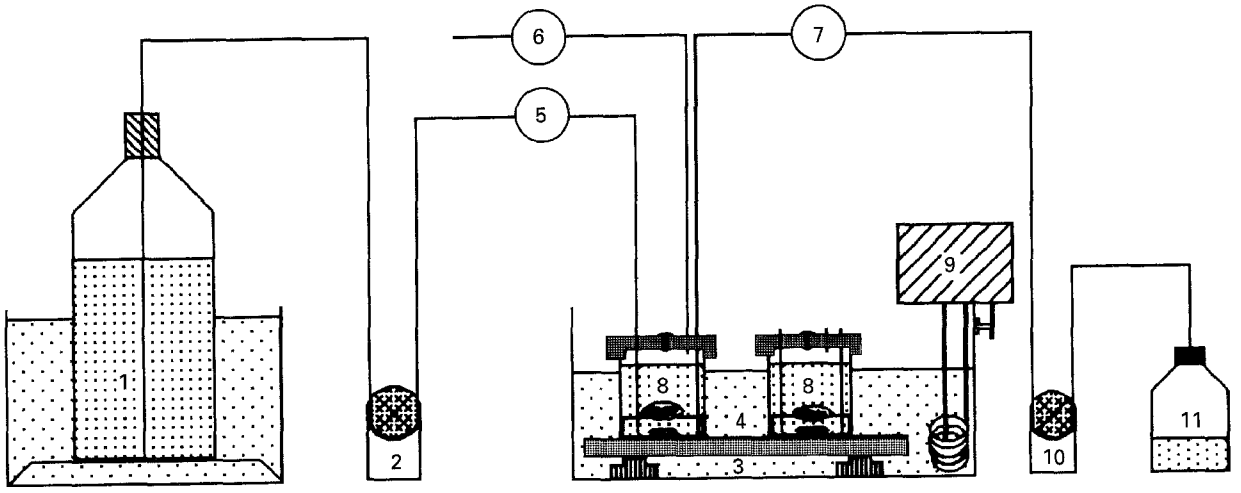

Figure 1 Experimental device used for the leaching of the glass fibres with periodic refilling of the reactor. 1, supply container; 2, peristaltic pump; 3, water bath; 4, magnetic stirrer; 5, filling valve; 6, venting valve; 7, draining valve; 8, reactors with glass fibres; 9, immersed circulator; 10, draining pump; 11, collection flask.

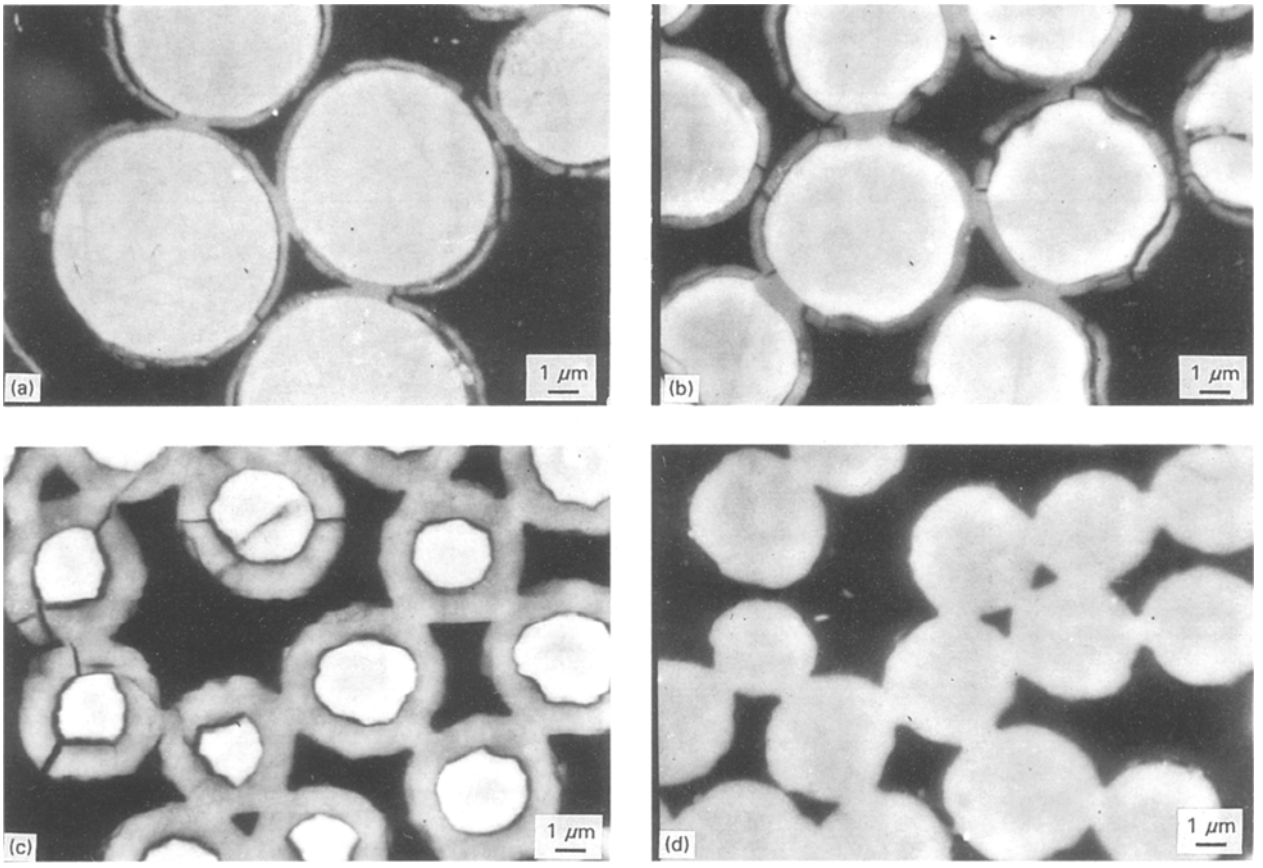

Figure 2 SEM backscattered electron images of the glass fibres, after various times of reaction and for different leaching modes, showing the unaltered core and the outer hydrated layer. (a) Static mode, $t = 3$ days; (b) stirred solution, renewed 24 times a day, $t = 3$ days; (c) stirred solution, renewed 72 times a day, $t = 3$ days; (d) stirred solution, renewed 24 times a day, $t = 10$ days.

mode (Fig. 2b and c). Finally, the unaltered circular core disappeared after 21 days in static conditions and 7–14 days during the runs with periodic refilling of the reactor (Fig. 2d). On the other hand, we have to underline that when using conditions of continuous leaching, other behaviour may be observed with formation of hollow tubes [31].

3.3. Weight losses

The dissolution kinetics of CM44 glass fibres, as monitored by relative weight losses curves, are shown in Fig. 3. Firstly, we notice that the weight loss reaches a constant value of 90% for the static mode experiments (21, 28 and 60 days) whereas it reaches 100% for the runs with periodic renewal of the solution. Moreover, Fig. 3 shows that, for the same leaching duration, the shorter is the cycle, the higher is the weight loss. We also notice that experiments with three renewals per day give similar results either with or without stirring of the solution.

Table III indicates for different durations of leaching: (i) the values of the weight losses, (ii) some values of the weight losses calculated from the chemical analysis of the dissolved silica assuming a congruent dissolution of the glass, and (iii) values deduced from the bulk radius of the fibres observed by SEM. The agreement between these results in good in spite of several discrepancies assigned to the composition and the density of the hydrated layer, which are different from

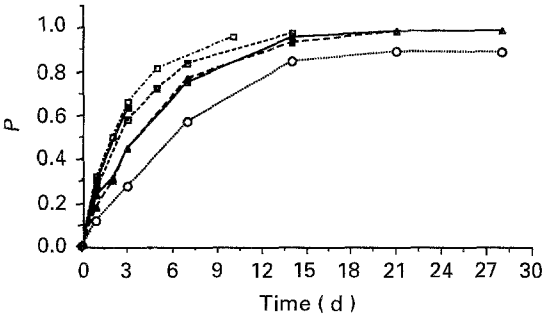

Figure 3 Relative weight loss, p, of the glass fibres versus time for different leaching modes. ST, static mode; R, periodic refilling mode; A, stirred solution; x in R(x) or RA(x) is the frequency of the refilling of the reactor in cycles per day. (○) ST, (△) R(3), (▲) RA(3), (⊡) RA(9), (□) RA(24), (■) RA(72).

those of the glass, and a certain heterogeneity of the diameters of the fibres before and after dissolution.

3.4. Chemical composition of the hydrated layer

The XPS analysis gives the surface composition of the outer part of the hydrated layer (depth of analysis $< 10^{-8}$ m) whereas the EDS analysis gives the mean composition of the hydrated layer at higher depth (about 10^{-6} m with respect to the accelerating voltage). Both XPS and EDS analysis data indicate that the residual hydrated layer, which is essentially

TABLE III Comparison between the weight losses (%) after different duration of leaching: (a) determined by weighing, (b) calculated from dissolved silica and (c) deduced from the fibre radius observed by SEM. ST, static mode; R(3), renewed three times a day; RA(x), stirred solution, renewed x times a day

Time (days)	ST			R(3)		RA(3)		RA(9)		RA(24)	
	(a)	(b)	(c)	(a)	(c)	(a)	(c)	(a)	(c)	(a)	(c)
1	11.7	nd	nd	17.7	19.0	23.7	ned	26.3	21.3	32.0	31.1
2	nd[a]	nd	nd	30.0	nd	31.4	nd	nd	nd	50.3	59.5
3	27.8	26.9	24.7	45.0	39.5	45.3	36.0	57.2	59.6	66.0	69.8
5	46.7	nd	nd	66.1	nd	nd	nd	72.0	69.5	81.7	82.4
7	54.8	50.8	45.3	77.3	73.2	75.2	nd	84.0	nd	nd	nd
14	83.2	76.7	83.8	94.2	83.8	96.7	84.0	98.3	99.6	96.6[b]	96.0[b]
21	90.0	90.0	84.0	99.8	96.0	99.8	nd	nd	nd	nd	nd
28	90.1	90.0	84.0	nd	nd	nd	nd	nd	nd	nd	nd

[a] nd, not determined.
[b] Run at 10 days.

TABLE IV Comparison between the Na/Si atomic ratios: (a) determined at the surface of the hydrated layer by XPS, (b) of the hydrated layer determined by EDS

Time (days)	ST		R(3)		RA(3)		RA(9)		RA(24)		RA(72)	
	(a)	(b)	(a)	(b)	(a)	(b)	(a)	(b)	(a)	(b)	(a)	(b)
3	0.24	nd	0.22	0.17	0.20	nd	0.14	nd	0.21	0.06	0.13	0.04
5	nd[a]	nd	nd	nd	nd	nd	0.23	0.03	0.14	0.06	nd	nd
7	0.21	nd	0.22	0.05	0.22	0.06	nd	0.01	nd	0.02[b]	nd	nd
14	0.19	0.04	nd	0.28	0.16	0.37	nd	0.01	nd	nd	nd	nd
21	0.18	0.11	nd	0.19	nd	0.11	nd	nd	nd	nd	nd	nd
28	0.19	0.01	nd	nd	nd	nd	nd	nd	nd	nd	nd	nd

[a] nd, not determined.
[b] Run at 10 days.

TABLE V Comparison between the Al/Si atomic ratios: (a) determined at the surface of the hydrated layer by XPS, (b) of the hydrated layer. ST, static mode; R(3), renewed three times a day; RA(x), stirred solution, renewed x times a day

Time (days)	ST		R(3)		RA(3)		RA(9)		RA(24)		RA(72)	
	(a)	(b)	(a)	(b)	(a)	(b)	(a)	(b)	(a)	(b)	(a)	(b)
3	0.15	nd[a]	0.16	0.05	0.24	nd	0.19	nd	0.21	0.10	0.17	0.05
5	nd	nd	nd	nd	nd	nd	0.24	0.15	0.20	0.15	nd	nd
7	0.18	nd	0.22	0.12[b]	0.23	0.11[b]	nd	0.15	nd	0.02[c]	nd	nd
14	0.17	0.20	nd	0.12	0.27	0.12[b]	nd	0.15	nd	nd	nd	nd
21	0.22	0.20	nd	0.23	nd	0.17	nd	nd	nd	nd	nd	nd
28	0.24	0.17	nd	nd	nd	nd	nd	nd	nd	nd	nd	nd

[a] nd, not determined.
[b] Analysis in part of the fresh glass determined by EDS.
[c] Run at 10 days.

siliceous, is strongly enriched in aluminium. On the other hand, XPS analysis shows that sodium is present at the leached layer–solution interface while EDS gives a negligible sodium concentration. Tables IV and V indicate the composition of the hydrated layer as Na/Si and Al/Si atomic ratios. Most samples exhibit an Al/Si atomic ratio of about 0.2 in contrast with 0.02 for the original glass.

These data, resulting from investigations at different scales, strongly suggest that the Al/Si ratio is constant in the hydrated layer. Therefore, even if hydration variations exist from inside to outside, the composition of the hydrated layer may be assumed to be homogeneous for SiO_2 and Al_2O_3 contents.

4. Interpretations

4.1. Dissolution progression

The observed morphologies of the fibres leads to the dissolution sketch (Fig. 4), that was previously described by Scholze and Conradt [7], as long as a fibre glass core is present.

In this study, we used the dimensionless parameters $z_1 = r_1/r_0$ and $z_2 = r_2/r_0$ to characterize the dissolution progress of the altered glass fibres, where r_1 is the radius of the unaltered core, r_2 the bulk radius and r_0 the mean radius of the initial glass fibres (i.e. 5 ± 0.5 μm). In a first approximation and taking into account the cylindrical shape of the fibres during their dissolution, we have (see Appendix 1)

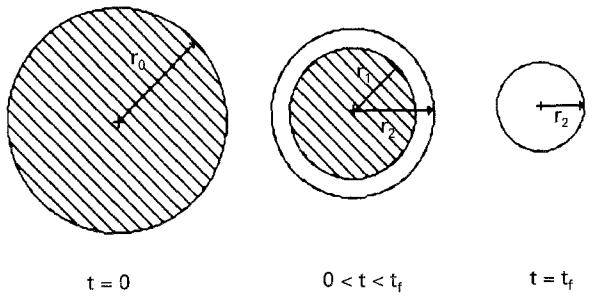

Figure 4 Sketch of the effects of the dissolution for a glass fibre. r_0, radius of the initial fibre; r_1, radius of the unaltered core; e, thickness of the outer hydrated layer; r_2, bulk radius ($r_2 = r_1 + e$). At time $t = t_f$, the unaltered core of the glass fibre has completely disappeared ($r_1 = 0$ and $r_2 = e$).

$$z_1 = \frac{r_1}{r_0} = (1 - \beta p)^{1/2} \quad (1)$$

with

$$p = \frac{m_0 - m_t}{m_0} \quad (2)$$

where p is the relative weight loss, m_0 the initial weight of the glass fibres (g), m_t the weight of glass fibres at time t (g) and β a dimensionless parameter whose value can be determined from experiments under static conditions (see Appendix 2).

The dissolution velocity of the glass at the unaltered core–hydrated layer interface, v_1 ($\mu m\, d^{-1}$), is calculated from Equation 1 by

$$v_1 = -r_0 \frac{dz_1}{dt} \quad (3)$$

The kinetic curves of the glass fibres dissolution are displayed as $z_1 = f(t)$ in Fig. 5 for the static and periodic refilling modes with a fixed value of β at 1.11. In this representation, a straight line reflects a constant dissolution velocity; actually, the curves present a slight curvature indicating a slowing down of v_1 with time. Estimating the initial dissolution velocity, v_0, from the tangent to the experimental curves at $t = 0$, we find respectively for runs ST, R(3), RA(3), RA(9), RA(24) and RA(72), $v_0 = 0.3$, 0.5, 0.6, 0.7, 0.9 and 0.9 $\mu m\, d^{-1}$, higher refilling frequencies leading to higher initial dissolution velocities with an asymptotic upper value.

4.2. Relation between the hydrated layer thickness and the dissolution progress

On the one hand, aluminium concentrations in the solutions are below the detection limit by AAS with a graphite furnace (i.e. < 10 p.p.b.); on the other hand, the XPS and EDS analyses give a nearly constant Al/Si atomic ratio of 0.2 in the hydrated layer. These results strongly suggest that the thickness of this layer only depends on the aluminium amount available from the glass after leaching. Under these conditions, a mass-balance calculation leads to determination of

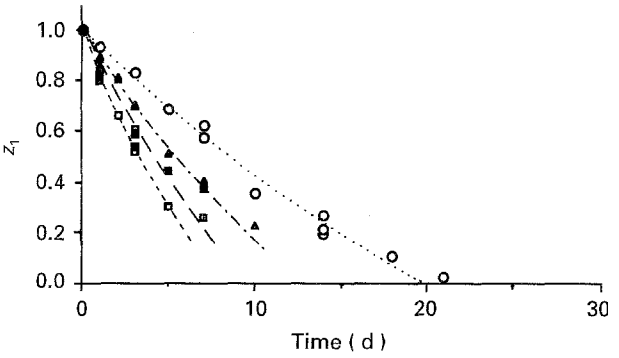

Figure 5 Dissolution kinetics of the glass fibres either with or without refilling of the reactor. The parameter z_1 is calculated from the relative weight loss with Equation 1 ($\beta = 1.11$). (○) ST, (△) R(3), (▲)RA(3), (⊡) RA(9), (□) RA(24), (■) RA(72).

the hydrated layer thickness, e, as a function of the dissolution progress, using assumptions of the water content and the density of the hydrated layer (see Appendix 1).

With such a model the calculated relative thickness, $z_h = e/r_0$, is expressed as

$$z_h = [1 - \gamma(1 - z_1^2)]^{1/2} - z_1 \quad (4)$$

with

$$\gamma = 1 - \alpha \frac{\rho}{\rho_h} \quad (5)$$

where e is the thickness of the hydrated layer (μm), ρ the unaltered glass density ($g\, \mu m^{-3}$), ρ_h the hydrated layer density ($g\, \mu m^{-3}$) and α the formation coefficient of the hydrated layer, i.e. the mass of the hydrated layer (g) per gram of dissolved glass.

The parameter α can be deduced from β (see Appendix 2) or calculated from the composition of the hydrated layer. The latter is assumed to be essentially an hydrated gel of SiO_2 and Al_2O_3 with a Si/Al atomic ratio of 5. This compound may have, for one mole of Al_2O_3, a molecular formula such as [10 SiO_2–Al_2O_3–nH_2O] with a molecular weight, M, of $702 + 18n$ g. The value of n has been determined with an electrobalance by heating up to 500 °C fully hydrated glasses (after 28 days dissolution in static conditions). This experiment suggests 16–19 mol H_2O per mol Al_2O_3, which implies $M = 990$–1044 g.

Taking into account the concentration in alumina ($c_a = 1\%$) of the anhydrous glass and the molecular weight of alumina ($M_a = 102$ g), we find

$$\alpha = c_a \frac{M}{M_a} \quad (6)$$

The value of the parameter α calculated in this way ($\alpha = 0.097$–0.102) is in excellent agreement with that deduced from β and the weight losses of the static mode experiments ($\alpha = 0.10$).

To determine the parameter γ, Equation 4 was fitted by a non-linear least squares method, to the thickness of the outer hydrated layer, e, and the relative radius of the unaltered core, z_1, both determined from SEM observations on polished sections of fibres.

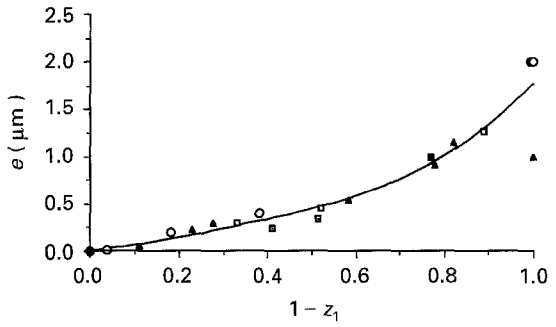

Figure 6 Thickness of the outer hydrated layer versus the relative radius of the unaltered core observed with SEM. The curve is fitted to the SEM data with Equation 4 by the non-linear least squares method. (○) ST, (△) R(3), (▲) RA(3), (⊡) RA(9), (□) RA(24), (■) RA(72).

This calculation gives a value of 0.875 for the parameter γ. The fitted curve $e = f(z_1)$ is shown in Fig. 6 with, in addition, the experimental plots.

The mathematical model fits well with the experimental data which are scattered close to the calculated curve whatever the experimental conditions. This good agreement strongly supports the validity of our previous assumptions about the composition of the hydrated layer.

When $z_1 = 0$, i.e. when the glass core has completely vanished, at time t_f the calculated thickness of the outer hydrated layer from Equation 4 (see Appendix 2) is $e = 1.8$ μm in good agreement, taking into account the difficulties to obtain a good sample at this step of reaction, with SEM data for static runs ($e = 2.0 \pm 0.2$ μm). In addition, a smaller value, $e = 1.0$ μm, measured for one experiment in periodic refilling mode when $t > t_f$, is reported as an example in Fig. 6.

4.3. Modelling

To model the dissolution of the glass fibre core, we have to account for two major results described earlier. Firstly the decreasing of the dissolution velocity with time and secondly the correlation between the initial dissolution velocity and the frequency of the renewal with a fresh solution.

Three factors may result in a slackening of the dissolution velocity: (i) the accumulation of the dissolved ions in the bulk of the solution controlling the rate of a surface reaction, (ii) a significant dispersion of the fibres diameters, and (iii) a diffusion-controlled mobility of the leached ions through the outer layer. The first explanation is classically invoked but a similar decreasing is also observed when the reactor is periodically refilled by the fresh solution. The distribution of fibre diameters leads to a slight variation with respect to a straight line when z_1 is small, but we think that the major part of the curvature is due to retardation by diffusion of the dissolved species through the outer layer. Thus, we propose a linear decreasing of the dissolution velocity in relation to the relative radius z_1, which is a geometric variable, rather than time

$$v_1 = v_0 u \tag{7}$$

with $u = 1 - k(1 - z_1)$ and $du = k dz_1$, where v_0 is the initial dissolution velocity ($t = 0$) (μm d^{-1}) and k a dimensionless parameter. Combining Equations 3 and 7

$$v_0 u = -\frac{r_0}{k}\frac{du}{dt} \tag{8}$$

The integration of the differential Equation 8 gives

$$z_1 = 1 - \frac{1}{k}\left[1 - \exp\left(-\frac{kv_0}{r_0}t\right)\right] \tag{9}$$

Equation 9 describes the variation of z_1 versus time only for static experiments. When the solution is periodically renewed at different frequencies, we have to consider a second component of the dissolution velocity, v_c, to explain the curves obtained in these conditions. We assume that v_c, on the one hand, depends on the thickness of the outer layer through u and, on the other hand, is rapidly decreasing with time. These assumptions lead to the expression

$$v_c = v_i u \exp(-k_c\theta) \tag{10}$$

where v_i is the initial velocity for the first renewal (μm d^{-1}), k_c a constant (d^{-1}) and θ the time (d) since the last refilling.

Thus, for a renewal cycle, the differential equation describing the dissolution velocity is expressed as

$$v_0 u + v_i u \exp(-k_c\theta) = -\frac{r_0}{k}\frac{du}{d\theta} \tag{11}$$

The integration of Equation 11 gives

$$z_1 = 1 - \frac{1}{k}\left\{1 - K\exp\left[-\frac{kv_0}{r_0}\theta + \frac{kv_i}{k_c r_0}\exp(-k_c\theta)\right]\right\} \tag{12}$$

where K is a constant which may be determined at each step by continuity of the geometric variable z_1 for $\theta = 0$.

The two parameters v_0 and k were calculated by fitting Equation 9 to the values of z_1, obtained for static experiments, with non-linear least squares method. Eventually, Fig. 7 shows that the theoretical

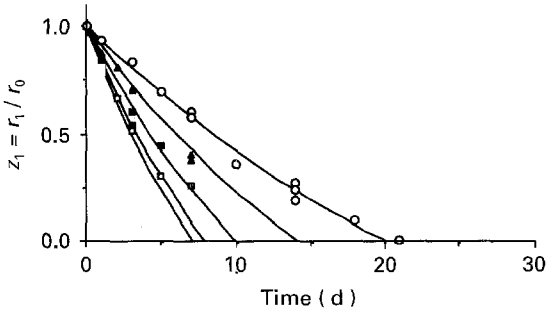

Figure 7 Modelling of the dissolution kinetics. The curve related to static experiments is fitted to the experimental data with Equation 9 by the non-linear least squares method. The curves related to the periodic refilling mode were graphically fitted to the experimental data with Equation 12. (○) ST, (△) R(3), (▲) RA(3), (⊡), RA(9), (□) RA(24), (■)RA(72).

model fits well to the data. The calculation indicates that the initial dissolution velocity, $v_0 = 0.34\ \mu m\ d^{-1}$ is approximatively halved ($k = 0.49$) when z_1 is near zero. The other two parameters, v_c and k_c, were graphically estimated from the data of the periodic refilling mode and Equation 12. The curves calculated with $v_c = 0.7\ \mu m\ d^{-1}$ and $k_c = 15\ d^{-1}$ were plotted in Fig. 7 for the renewal frequencies of 3, 9, 24 and 72 cycles d^{-1} (i.e. $\theta_{max} = 8$ h, 2 h 40 min, 1 h, and 20 min). The fit between the theoretical model and all the data, whatever the leaching conditions, is good. This agreement supports our assumptions of the accelerating effect at each renewal with a fresh solution. Furthermore, our model is compatible with a limit for the dissolution velocity ($v = v_0 + v_c$) at an "infinite" renewal frequency as suggested by runs at 72 cycles d^{-1}.

4.4. Dissolution mechanism

After a short induction period, the glass–solution reaction involves a selective dissolution of the glass modifiers, sodium, calcium and magnesium. Boron is also easily dissolved, breaking down the network of the glass. Finally, all the components of the glass are leached except aluminium and a part of silicon. These two elements accumulate within the outer hydrated layer in the Al/Si atomic ratio of 0.2. The leached species diffuse through the outer gel of SiO_2 and Al_2O_3 to the saline solution. The increase of the thickness of the hydrated layer with time results in a slight decrease of the dissolution velocity at the unaltered glass–hydrated layer interface.

Under static conditions the dissolution of the glass proceeds up to the complete dissolution of the fibre material. At this state ($t = t_f$), the bulk dissolution is apparently stopped ($p = 90\%$ at 21, 28 and 60 d).

For all the runs with periodic refilling of the reactor, two essential differences occur: (i) the dissolution velocity is greater for the first runs, (ii) the glass fibres are finally entirely dissolved, including the outer hydrated layer.

A possible explanation is that, at each supply with the fresh solution, the concentration of the solution in silicon and aluminium at the outer layer–solution interface drastically drops. As a result of these low concentrations there is a limited solubilization of the hydrated layer and mostly an acceleration of the reaction rate at the unaltered glass–hydrated layer interface.

Additional experiments (in progress), with variable silica contents in the bulk solution, suggest a rapid transfer of SiO_2 by diffusion through the outer layer. Accordingly this process is not rate-limiting. An alternative explanation is, at each supply of fresh solution, an increase of the concentration of a species involved in the hydration process (e.g. the hydronium species) and its rapid diffusion to the hydrated front.

Whatever the exact mechanism, after the complete dissolution of the fibre material ($t > t_f$), the aluminium liberated during the dissolution of a part of the hydrated layer, at each renewal with the fresh solution, remains in the saline solution because the source of silica at the unaltered glass–hydrated layer interface no longer exists. The hydrated silico-aluminous residue is then in part dissolved at each renewal until complete dissolution.

Our explanation supposes a mobility of all the components of the hydrated layer which is compatible with the fact that the boundaries of the layer are moving. On the other hand, it seems that the limiting factor for the glass dissolution is really the solubility of the silico-aluminous gel. *In vivo*, the concentrations in silicon and aluminium of the leaching solution are probably negligible; this is propicious to the clearance of the fibres.

5. Conclusions

1. The selective dissolution of glass fibres in a physiological saline solution leads to the formation of an outer hydrated layer easily characterized by SEM–EDS and XPS. It occurs under non-steady-state conditions and the total transformation of the fresh core is finally observed. As far as this selective dissolution proceeds, there is simultaneously a decrease of the diameter of the bulk fibre and an increase of the thickness of the leached layer.

2. Using thermogravimetric analysis, SEM–EDS and XPS, the composition of the hydrated layer may be supposed to be homogeneous. An approximate composition is as follows: $10\ SiO_2 \cdot Al_2O_3 \cdot 16\text{–}19\ H_2O$. The lack of detectable aluminium in leaching solutions, combined to the constant composition of the layer, implies a direct proportionality between the mass of the hydrated layer formed and the mass of silica released at the unaltered core–outer layer interface. A theoretical relation (Equation 4) between z_1, the relative radius of the unaltered core and the thickness, e, of the hydrated layer may be established.

The good agreement with experimental data (Fig. 6) pleads for the validity of the different assumptions supporting Equation 4.

3. Dissolution kinetics has been investigated either without or with periodic refilling of the reactor at variable frequencies (3, 9, 24 and 72 cycles d^{-1}). Dissolution rates are directly correlated to the frequency of refilling, the higher ones corresponding to the higher dissolution rates. An extrapolation to the "infinite refilling frequency" is possible (Fig. 5).

4. Bulk dissolution of the fibres results both from the selective dissolution of the fibre material associated to the formation of the leached layer (and possibly its dissolution). This layer may be vizualized as a gel-like product sticking on to the glass core. The diameter reduction of the unaltered glass core necessarily leads to re-organizations within the alumino-silica gel. Accordingly, selective dissolution appears to be the dominant process as long as fresh glass is still present.

A possible explanation of the relation between frequencies of refilling and dissolution rates is as follows. The accumulation of silica in the solution near the fibres is supposed to slow down the diffusion of dissolved SiO_2 through the porosity of the gel layer. The rapid drop related to solution renewal results in a steeper silica gradient and hence an acceleration of

the selective dissolution. Alternatively, one may invoke the rapid diffusion of a reactive species (e.g. H_3O^+) periodically supplied at each refilling to the hydration front. By contrast, when the fresh glass has disappeared, the silica source is exhausted and congruent dissolution of the gel may proceed at a more significant rate.

Acknowledgements

The authors thank Professor F. Cesbron for his keen interest and help for TGA measurements and Saint-Gobain Recherche (Aubervilliers, France) for collaboration and supply of glass fibres.

Appendix 1. Relations between the mass loss and the geometrical coordinates of the leached fibre

Considering a unique fibre glass at time $t = 0$, the initial volume, V_0, and mass m_0, are:

$$V_0 = \pi r_0^2 l \quad \text{(A1)}$$

$$m_0 = \rho V_0 \quad \text{(A2)}$$

where r_0 is the mean initial radius (μm), ρ the density of the glass (g μm^{-3}) and l the length of the fibre (μm).

At time t, we assume that the unaltered core of radius, r_1, is surrounded by an outer layer of thickness, e, as shown schematically in Fig. 4. The bulk radius, r_2, is

$$r_2 = r_1 + e$$

The volume of the unaltered core, V_1, is

$$V_1 = \pi r_1^2 l = z_1^2 V_0 \quad \text{(A3)}$$

with $z_1 = r_1/r_0$.

The volume of the outer layer, V_h, is

$$V_h = \pi r_2^2 l - \pi r_1^2 l$$

$$= (z_2^2 - z_1^2) V_0 \quad \text{(A4)}$$

with $z_2 = r_2/r_0$.

The corresponding masses, m_1 and m_h, are

$$m_1 = \rho V_1 = m_0 z_1^2 \quad \text{(A5)}$$

$$m_h = \rho_h V_h = m_0 \frac{\rho_h}{\rho}(z_2^2 - z_1^2) \quad \text{(A6)}$$

where ρ_h is the density of the hydrated outer layer (g μm^{-3}).

At time t, the relative weight loss, p, is calculated from the difference between the initial weight and the weight at time t, divided by the initial value

$$p = \frac{m_0 - (m_1 + m_h)}{m_0}$$

$$p = 1 - z_1^2 - \frac{\rho_h}{\rho}(z_2^2 - z_1^2) \quad \text{(A7)}$$

On the other hand, the mass of the hydrated outer layer can be calculated from the quantity of the aluminium liberated during the dissolution of the glass if we neglect the aluminium in solution. Under these conditions, the mass of the layer is proportional to the difference between the initial mass and the mass of the unaltered core

$$m_h = \alpha(m_0 - m_1) \quad \text{(A8)}$$

where α is a dimensionless constant which represents the mass of the hydrated layer per gram of dissolved glass.

From Equations A8, A5 and A2 we have

$$V_h = \alpha \frac{\rho}{\rho_h}(1 - z_1^2) V_0 \quad \text{(A9)}$$

Combining Equations A4 and A9 gives

$$\alpha \frac{\rho}{\rho_h}(1 - z_1^2) = z_2^2 - z_1^2 \quad \text{(A10)}$$

Combining Equations A7 and A10 leads to an expression for the weight loss only depending on z_1

$$p = (1 - \alpha)(1 - z_1^2) \quad \text{(A11)}$$

Conversely, the relative radius of the unaltered core z_1 is related to the weight loss p by

$$z_1 = (1 - \beta p)^{1/2} \quad \text{(A12)}$$

with $\beta = 1/(1 - \alpha)$. The relative bulk radius z_2 is expressed as z_1 from Equation A10 by

$$z_2 = [1 - \gamma(1 - z_1^2)]^{1/2} \quad \text{(A13)}$$

with

$$\gamma = \left(1 - \alpha \frac{\rho}{\rho_h}\right) \quad \text{(A14)}$$

Finally, the relative thickness ($z_h = e/r_0$) of the outer hydrated layer can be only expressed as z_1 by

$$z_h = z_2 - z_1$$

$$= [1 - \gamma(1 - z_1^2)]^{1/2} - z_1 \quad \text{(A15)}$$

Appendix 2. Determination of the value of the parameters α, β, γ and ρ_h

At time $t = t_f$, when the unaltered core completely disappeared we have $z_1 = 0$ and $z_2 = z_h$. The parameter β can be estimated from the plateau value ($p = 0.9$) obtained in static mode experiments for $t \geq t_f$ and Equation A12

$$\beta = \frac{1}{p} = 1.11 \quad \text{(A16)}$$

α can be simply deduced from β

$$\alpha = 1 - \frac{1}{\beta}$$

$$= 0.1 \quad \text{(A17)}$$

The parameter γ is calculated by fitting Equation A15 ($z_h = f(z_1)$) to the SEM data for $t \leq t_f$. We find $\gamma = 0.875$.

Finally ρ_h is deduced from γ by

$$\rho_h = \frac{\alpha\rho}{1 - \gamma} \tag{A18}$$

with $\rho = 2.5 \times 10^{12}\,\mathrm{g\,\mu m^{-3}}$ we find $\rho_h = 2.0 \times 10^{12}\,\mathrm{g\,\mu m^{-3}}$.

References

1. H. SCHOLZE, *Glastech. Ber.* **61** (1988) 161.
2. R. M. POTTER and S. M. MATTSON, *ibid.* **64** (1991) 16.
3. S. M. MATTSON, *Environ. Health Perspectives* **102**, supp. 5 (1994) 87.
4. J. C. TOURAY and P. BAILLIF, *ibid.* **102**, supp. 5 (1994) 25.
5. P. BAILLIF and J. C. TOURAY, *ibid.* **102**, supp. 5 (1994) 77.
6. S. THELOHAN and A. de MERINGO, *ibid.* **102**, supp. 5 (1994) 91.
7. H. SCHOLZE and R. CONRADT, *Ann. Occup. Hyg.* **31** (1987) 683.
8. H. FÖRSTER and H. TJESLER, *Glastech. Ber.* **66** (1993) 255.
9. B. CHOUIKHI, P. BAILLIF and J. C. TOURAY, *C. R. Acad. Sci. Paris* **318** série II (1994) 1051.
10. A. PAUL, "Chemistry of glasses" (Chapman and Hall, New York, 1982).
11. J. ZARZYCKI, "Les verres et l'état vitreux" (Masson, Paris, 1982).
12. B. M. J. SMETS, *Philips Tech. Rev.* **42** (1985) 59.
13. J. L. CROVISIER, J. HONNOREZ and J. P. EBERHART, *Geochim. Cosmochim. Acta* **51** (1987) 2977.
14. K. G. KNAUSS and T. J. WOLERY, *ibid.* **52** (1988) 43.
15. C. AMRHEIN and D. L. SUAREZ, *ibid.* **52** (1988) 2785.
16. L. L. HENCH, *J. Non-Cryst. Solids* **19** (1975) 27.
17. F. R. BACON, *Glass Ind.* **49** (1968) 483.
18. W. A. LANFORD, K. DAVIS, P. LAMARCHE, T. LAURSEN, R. GROLEAU and R. H. DOREMUS, *J. Non-Cryst. Solids* **33** (1979) 249.
19. W. SMIT and H. S. STEIN, *ibid.* **34** (1979) 357.
20. T. ADVOCAT, PhD thesis, University Louis Pasteur, Strasbourg, France (1991).
21. C. GUY, PhD thesis, University Paul Sabatier, Toulouse, France (1989).
22. J. V. WALTER and H. C. HELGESON, *Am. J. Sci.* **277** (1977) 1351.
23. P. AAGAARD and H. C. HELGESON, *ibid.* **282** (1982) 237.
24. H. C. HELGESON, W. M. MURPHY and P. AAGAARD, *Geochim. Cosmochim. Acta* **48** (1984) 2405.
25. W. M. MURPHY and H. C. HELGESON, *ibid.* **51** (1987) 3137.
26. A. C. LASAGA, in "Reviews of mineralogy", Vol. **8** (Mineralogical Society of America, Washington, 1983) 135.
27. J. L. GAMBLE, "Chemical anatomy, physiology and pathology of extracellular fluid", 8th Edn (Harvard University Press, Boston, 1967).
28. G. M. KANAPILY, O. G. RAABE, C. H. T. GOH and R. A. CHIMENTI *Health Phys.* **24** (1973) 497.
29. G. FECK, PhD thesis, Rheinisch-Westfälischen Technischen Hochschule, Aachen, Germany (1984).
30. J. P. LEINEWEBER, "Biological effects of man-made mineral fibres", Vol. 2 (World Health Organization, Copenhagen, 1984) p. 87.
31. B. CHOUIKHI, PhD thesis, University of Orléans, France (1995).

Received 26 July 1994
and accepted 7 June 1995